A Topology Morphing Partial Power Converter with Variable Turns Ratio for Integration of On-Board Battery Chargers with DC Buildings

Niwton Gabriel Feliciani dos Santos, Andrii Chub
Power Electronics Group of TalTech
Tallinn University of Technology (TalTech)
Tallinn, Harjumaa, Estonia
niwton.feliciani@taltech.ee, andrii.chub@taltech.ee

Mário Lúcio da Silva Martins
Power Electronics and Control Research Group
Federal University of Santa Maria (UFSM)
Santa Maria, RS, Brazil
mario-lucio.martins@ufsm.br

***Abstract*—This paper proposes a step-up/down series-connected partial power converter (S-PPC) with variable turns ratio for the dc–dc stage of an on-board charger (OBC), introducing a feature that enables the selection between (i) conventional slow charging through the ac grid or (ii) the integration with dc buildings. For both cases, the S-PPC employs a three-leg switch configuration to morph its transformer primary winding and achieve three different turns ratios, which are designed to reduce the circulating currents during most of the charging mode. In addition, the soft-switching operation also contributes to enabling the proposed S-PPC to operate in a relatively wide voltage gain range with high performance. The simulation results are in agreement with and validate the analysis presented in this paper.**

***Index Terms*—DC building, on-board charger (OBC), partial power processing (PPP), soft-switching, variable turns ratio.**

I. Introduction

THE rapid proliferation of battery electric vehicles (EVs) has driven innovation in the technologies for EV chargers and powertrain systems. Basically, the high-voltage battery pack of an EV is commonly charged conductively from a fast or semi-fast charging station (off-board) or the ac utility grid via an on-board charger (OBC) [1], and its voltage can vary in a wide operation range [2]. For off-board charging, the built-in OBC is bypassed because all the power is converted to dc outside an EV, as shown in Fig. 1 (path ③) [3]. In contrast, built-in OBCs are typically used to convert power from ac to dc inside an EV. They include a front-end power factor correction (PFC) ac–dc converter, followed by a dc–dc converter [4], with both converters sharing an intermediate dc bus.

With growing interest in dc power distribution for future energy-efficient buildings [5], it is extremely crucial to develop new OBCs that can be integrated with dc buildings. Hence, this paper proposes modifying conventional OBCs by adding only two relays to provide slow charging either from the ac grid (path ① in Fig. 1) or a dc building (path ②). It allows the dc–dc stage of the OBCs to be compatible with both charging methods without requiring an external converter, provided the converter can handle variations in both input and output voltages.

The partial power processing (PPP) concept has received considerable attention recently, including for EV charging applications, but its use in OBCs has not been fully investigated [4], [6]. Recent papers mainly focus on its use in EV powertrain [7], including those employing a hybrid energy storage system (HESS) [8], and in fast charging stations (FCSs) [9]. The core idea of PPP is that a PPP converter (PPC) processes only a small fraction of the total active power supplied to the system [10]. As the series-connected PPCs (S-PPCs) regulate the voltage difference between the input and output, the amount of power processed is proportional to the voltage regulation range (Δv). Therefore, their benefits are fully realized only when the voltage gain and its parameters – such as duty cycle, phase shift angle, turns ratio, and/or switching frequency – are properly designed [10], which requires restraining Δv as a fraction of the EV battery pack voltage range.

To overcome all challenges and achieve a good trade-off between power processing, performance, and voltage range, this paper proposes a series-input–parallel-output (SIPO) topology morphing S-PPC for the dc–dc stage highlighted in blue in Fig. 1. In short, it can reconfigure the connection of the transformer primary windings to achieve three selectable turns ratios for a wide output voltage regulation range. With proper design, it can operate predominantly with a configuration (Conf.) featuring a higher turns ratio, reducing the conversion effort on the dc–dc converter by minimizing circulating currents compared to the S-PPC based on a non-morphing topology.

II. Steady-State Evaluation of the SIPO S-PPC

Fig. 2 illustrates the circuit diagram of the proposed current-fed full-bridge/stacked asymmetrical half-bridge (CFFB/SAHB) SIPO S-PPC. As shown, the CFFB and SAHB circuits are coupled with a three-winding morphing transformer modeled

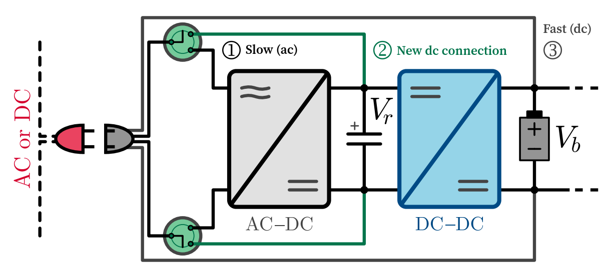

Fig. 1. Architecture of a $1-\phi$ OBC with the proposed modification to allow either ① conventional slow ac charging or ② integration with dc buildings.

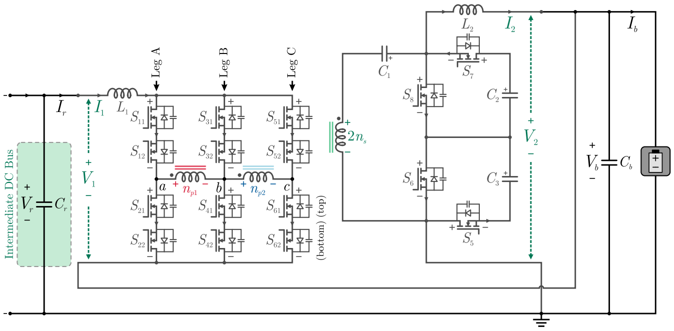

Fig. 2. Circuit diagram of the proposed CFFB/SAHB SIPO S-PPC.

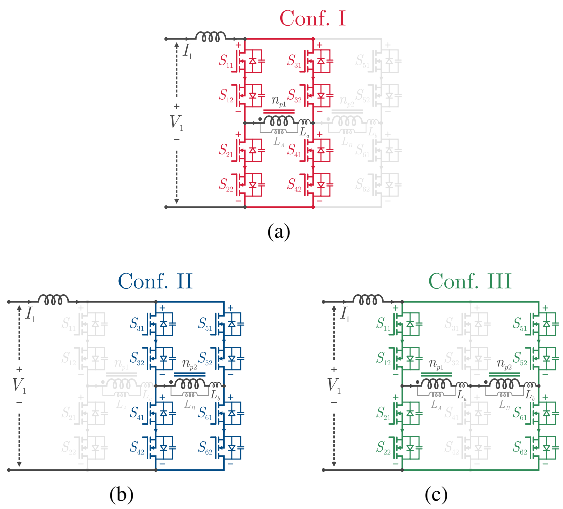

Fig. 3. Three configurations of the CFFB morphing circuit: (a) Conf. I (leg C OFF), (b) Conf. II (leg A OFF), and (c) Conf. III (leg B OFF).

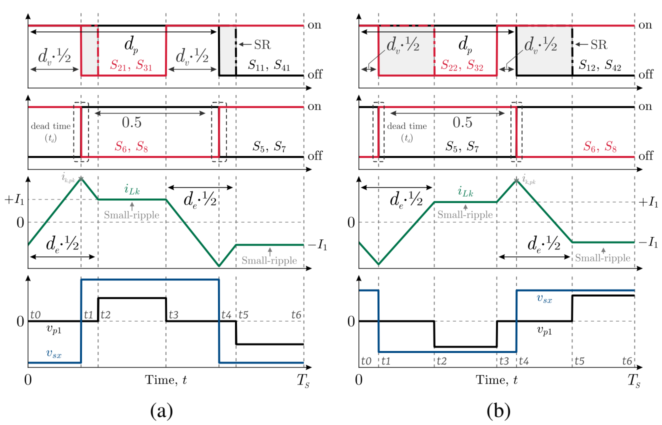

Fig. 4. Switching sequence and steady-state waveforms of the S-PPC in (a) step-down and (b) step-up modes (using Conf. I as an example).

with magnetizing (L_M) and leakage (L_k) inductances, referred to as the primary side. It provides the galvanic isolation required for the S-PPC to function properly, while the dc bus and the battery pack share the common ground [4].

The proposed morphing SIPO S-PPC is bidirectional, and it has the capability to step the system voltage up or down in both directions of power flow. The capability to support bidirectional active power flow enables it to facilitate vehicle-to-grid (V2G), vehicle-to-home (V2H), and vehicle-to-load (V2L) functionalities [11], which are a trend in the EV market and can be very useful for dc buildings. In addition, the presence of two filter inductors ensures a non-pulsating current with a low high-frequency ripple on both dc sides.

A. Operating Principles

Back-to-back switches serve two functions on the primary side: (i) enable operation within a bipolar voltage at the series port [10], ensuring four-quadrant operation capability, and (ii) select/morph the primary winding based on the voltage gain. The CFFB primary circuit can then operate in three different Confs., as shown in Fig. 3, allowing the transformer to exhibit three distinct turns ratios (n) and leakage inductances:

$$\begin{aligned} n_a &= \frac{n_s}{n_{p1}} \quad \text{and} \quad L_k = L_a \qquad \text{(Conf. I)},\\ n_b &= \frac{n_s}{n_{p2}} \quad \text{and} \quad L_k = L_b \qquad \text{(Conf. II)},\\ n_c &= \frac{n_s}{n_{p1}+n_{p2}} \quad \text{and} \quad L_k = L_a + L_b \qquad \text{(Conf. III)}. \end{aligned} \tag{1}$$

In Conf. I of the step-down mode, for example, the bottom primary switches remain turned ON during the entire switching period (T_S), i.e., the switching frequency (f_s) is $f_s = 1/T_S$, while the pulse-width modulation (PWM) is applied to the top switches following the pattern shown in Fig. 4(a). In this mode, the linkage between the PWM duty cycle (d_p), overlapping duty cycle (d_v), and effective duty cycle (d_e) is given by

$$d_p = \frac{(1+d_v)}{2}, \quad d_e = d_v + \delta, \quad \delta = d_v - \frac{16 n \varpi}{M_C}, \tag{2}$$

where ϖ is the normalized value of L_k and $M_C = V_2/V_1$.

In step-up mode, on the other hand, the top switches remain turn ON during the entire period, while the PWM is applied to the bottom switches following the pattern shown in Fig. 4(b). Here, d_p and d_e are the same as in (2), however

$$\delta = d_v + \frac{16 n \varpi}{M_C}. \tag{3}$$

In Fig. 4, dash-and-dot lines in the uppermost waveforms indicate the increment by which the width of the primary switch gate–source signals must be increased to implement synchronous rectification (SR), which reduces the conduction losses. The operation in either Conf. II or Conf. III is similar to that of Conf. I. Additionally, during discharging, the S-PPC transfers active power from the battery pack to the intermediate dc bus, operating similarly to the charging mode.

B. Soft-Switching Characteristics

Properly designed CFFB/SAHB SIPO S-PPC employing the PWM strategies depicted in Fig. 4 can achieve full-range zero-current switching (ZCS) naturally for all the primary switches without the need for lossy, bulky, and costly snubbers or active-clamp circuits to suppress the high turn-OFF voltage spikes across these switches. Such voltage spikes are common in isolated current-fed (CF) converters due to the inherent mismatch between the leakage (i_{Lk}) and input inductance (i_1) currents at the beginning of an active state, leading to increased

$$M_C = \frac{\pm 2\,n\left[1+\left(\{4\varpi-1\}^2+\{16\varpi+4\}\,\kappa\,d_v+4\,\kappa^2\{d_v^2-4\varphi\}\right)^{1/2}+2\,\kappa\,\{d_v-2\varphi\}\right]}{(1-2\,d_v)}, \quad \varpi=\frac{L_k\,f_s}{R_1}, \quad \varphi=\frac{L_1\,f_s}{R_1}, \quad \kappa=\frac{L_k}{L_1}, \quad R_1=\frac{V_1}{I_1}. \tag{6}$$

electromagnetic interference, reduced system reliability, and potential damage to the semiconductor devices. In the proposed SIPO S-PPC, the soft-switching effectively absorbs all the energy stored in the leakage inductance(s).

With the used modulation, the primary switches turn OFF with ZCS assisted with the conduction of their body diodes and turn ON with ZCS owing to the low rise rate of their currents (di/dt) [12]. In step-down mode, the top switches realize ZCS turn-OFF *only if* $|i_{Lk}| \geq |I_1|$ (considering small-ripple approximation) at the turn-OFF moments. These conditions allow the reverse current to flow through the body diodes and avoid the current mismatch between i_{Lk} and I_1 at t_1 and t_4, which is achievable by manipulating two constraints,

$$L_k \leq L_{cr}, \qquad \text{where} \quad L_{cr} = \frac{M_C\,d_v\,V_1}{16\,n\,f_s\,I_1}. \tag{4}$$

Generally, L_k is constant, while the duty cycle changes in response to the voltage gain. Therefore, for a given L_k,

$$d_v \geq \frac{16\,n\,\varpi}{M_C}. \tag{5}$$

To ensure ZCS for the primary switches in step-up mode, no specific conditions are required. Instead, only the following constraint must be satisfied: $d_v \geq 0$, because there are no scenarios that result in a current mismatch between i_{Lk} and I_1 at the turn-OFF moments. Hence, the high-voltage spikes are inherently avoided in step-up mode. Finally, the dead time (t_d) between the odd (S_5, S_7) and even (S_6, S_8) switches ensures their zero-voltage switching (ZVS) [12] in both step-down and step-up modes. Consequently, the proposed SIPO S-PPC can reduce or almost eliminate the switching losses.

C. Static Voltage Gain

By using the principle of volt-second balance applied to the L_1, the voltage gain V_2/V_1 can be derived as shown in (6), where "$\pm$" corresponds to "$+$" in step-down mode and "$-$" in step-up mode. The voltage gain of the dc–dc stage is

$$M = V_b/V_r = M_C/(1+M_C). \tag{7}$$

If $\kappa \approx 0$, M_C can be simplified and rewritten as

$$M_C = \frac{\pm 2\,n\,(1+|4\varpi-1|)}{(1-2\,d_v)}. \tag{8}$$

III. Case Study and Simulation Results

By considering the battery pack of the Nissan LEAF® and that the dc buildings should operate within the nominal voltage range of $320-380$ V [5], Fig. 5 shows the diagram of the operation points (OPs) of the CFFB/SAHB SIPO S-PPC along with the respective configurations. As can be seen, the variable turns ratio approach combined with the proper design of the three values of n allows the S-PPC to operate predominantly within an input and output voltage range where the transformer

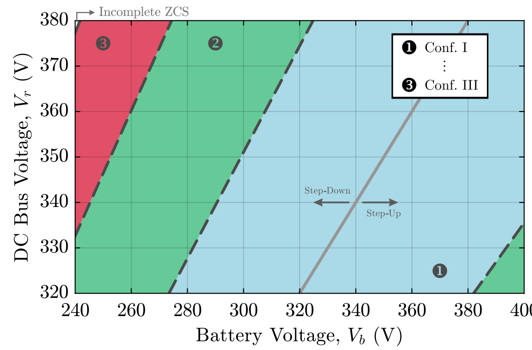

Fig. 5. Diagram of the OPs of the CFFB/SAHB S-PPC along with their respective Confs., considering variations in input and output voltages.

turns ratio is higher (Conf. I), which reduces conduction losses by minimizing the circulating currents.

In other words, the values of n and L_k have been chosen to cope with a wide voltage range, ensuring that the majority of the charging process occurs within a more advantageous range, extending it only when necessary. Another goal has been to ensure ZCS for all primary switches and ZVS for all secondary switches throughout the voltage range.

A. Turns Ratio Design Guidelines

In this design procedure for selecting the turns ratios, the following two constraints must be satisfied:

$$n_a > n_b > n_c, \qquad n_c = \frac{(n_a \times n_b)}{(n_a + n_b)}. \tag{9}$$

The turns ratio for Conf. I (n_a) has been designed to ensure its utilization in mostly step-up mode:

$$n_a \leq \frac{(2\,d_{v\_min}-1)\,M_C}{2\,(1+|4\,\varpi-1|)}, \tag{10}$$

where d_{v_min} is the minimum overlapping duty cycle selected by the designer to maintain $d_p > 0.5$.

Finally, the turns ratio for Conf. II (n_b) has been designed to ensure operation at $V_r = 320$ V and $V_b = 240$ V:

$$n_b \leq \frac{M_C\,d_{v\_min}}{16\,\varpi}. \tag{11}$$

Fig. 6 illustrates the root-mean-square (RMS) value of the leakage current (i_{Lk}), based on the values of n and L_k listed in Table I. In the case of the traditional (non-morphing) S-PPC, a larger voltage gain range results in a lower required value of n and a higher RMS leakage current (and circulating currents), which in turn leads to high conduction losses. In contrast, the proposed variable turns ratio approach enables the S-PPC to operate in a wide voltage range with low RMS currents by morphing the transformer primary winding to the optimal corresponding configuration at each operating point.

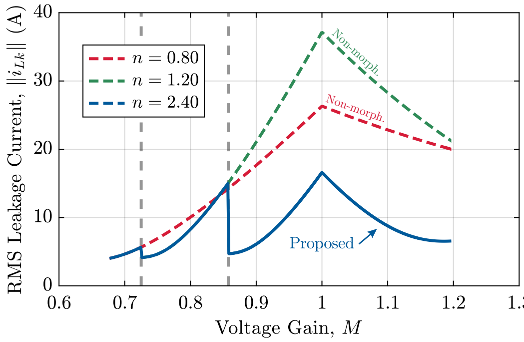

Fig. 6. RMS leakage current during the CC mode, employing the traditional-based non-morphing S-PPC and the proposed variable turns ratio approach.

TABLE I
SIMULATION PARAMETERS FOR THE CFFB/SAHB S-PPC

Parameter	Part	Parameter	Part	Parameter	Part
V_{CV}	373 V	f_s	50 kHz	n_a, L_a	$2.4, 12\ \mu$H
C_r, C_b	5 μF	$C_1 - C_3$	27 μF	n_b, L_b	$1.2, 11\ \mu$H
L_1	660 μH	L_2	3.2 mH	n_c, L_c	$0.8, 23\ \mu$H

B. Simulation Results

To validate the proposed CFFB/SAHB S-PPC, it has been simulated using the PSIM® software, where the parameters and components used are listed in Table I. The battery pack is modeled as a resistor (R_b) whose resistance is $R_b \approx 63\ \Omega$, but the EV battery pack is supposed to be charged using the conventional constant current/constant voltage (CC/CV) charging method, whose control block diagram is shown in Fig. 7 [4]. During discharging, a different control system must be used to meet the dc bus voltage and power demand.

Fig. 8(a) shows the waveforms at the input/output terminals and transformer windings. In this case, the morphing S-PPC operates in step-down mode (with $V_r = 325$ V, $V_b = 240$ V) with Conf. II. Similarly, Fig. 8(b) shows the waveforms at the same terminals but in step-up mode (with $V_r = 325$ V and $V_b = 373$ V) and Conf. I. The nominal power is 2.2 kW, and the dead time between the secondary switches is 600 ns. Finally, Fig. 9 illustrates the theoretical and circuit simulation results for the voltage gain of the proposed morphing SIPO S-PPC, considering two scenarios for the dc bus voltage during the CC charging mode: $V_r = 325$ V and $V_r = 375$ V. In these figures, the lines represent the analytical solutions for M_C (for $\kappa \approx 0$) and M, while the markers correspond to the simulation data, which closely match each other. When connected to a single-phase ac grid, the proposed S-PPC can charge the EV battery pack using the same dc bus voltage of $320-380$ V, but in this case, regulated by the PFC converter.

C. Comparative Analysis

Table II compares the CFFB/SAHB S-PPC to some morphing converters reported in the literature for EVs, which have been applied to OBCs [13], [14] and also FCSs [15], in terms of topology, modulation, and morphing capabilities, number of Confs., semiconductors, and transformers, soft-switching and partiality features, voltage and power levels, and f_s.

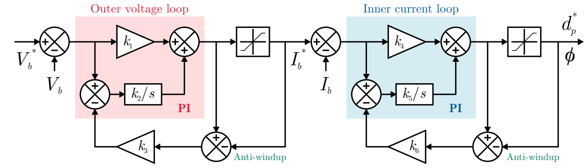

Fig. 7. Control block diagram of the CC/CV battery charging method [4].

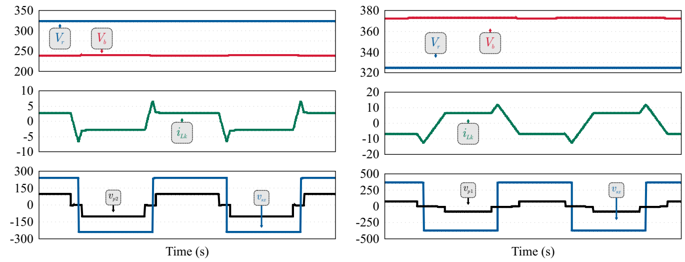

(a) (b)

Fig. 8. Simulation waveforms at the input and output terminals of the dc–dc stage and morphing transformer, for $V_r = 325$ V: (a) step-down mode and Conf. II, and (b) step-up mode and Conf. I.

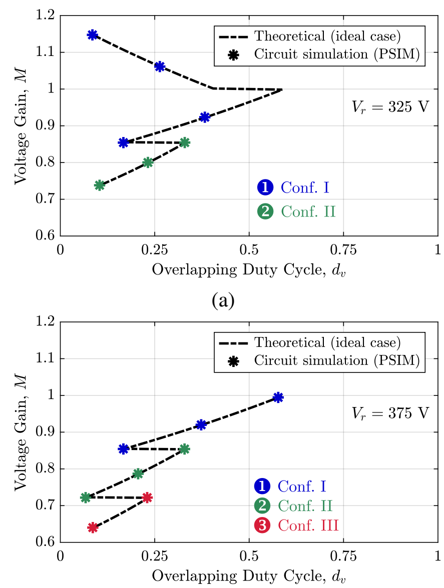

(a)

(b)

Fig. 9. Theoretical and circuit simulation results concerning the voltage gain of the CFFB/SAHB S-PPC, for (a) $V_r = 325$ V and (b) $V_r = 375$ V.

The most commonly used morphing topologies for EVs are based on resonant [2], [13], [14] and dual-active-bridge (DAB) converters [15], which typically involve morphing either the primary-side inverter, secondary-side rectifier, resonant tank, or transformer turns ratio. While the converters in [13] and [15] operate at a fixed frequency, as the CFFB/SAHB S-PPC, those in [2] and [14] use variable-frequency operation. All evaluated topologies offer three or four possible configurations, use a single transformer with two or three windings, and achieve soft-switching. Notably, only the CFFB/SAHB S-PPC performs PPP and has a non-pulsating current on both dc sides, and only it and the converter in [14] are bidirectional.

An emerging monolithic bidirectional (MBD) switches could greatly reduce the switch count in the proposed SIPO S-PPC

TABLE II
COMPARISON BETWEEN THE CFFB/SAHB SIPO S-PPC AND SOME MORPHING CONVERTERS FOR EV APPLICATIONS

Parameter	[15] 2023	[14] 2023	[13] 2025	Proposed
Topology	Semi-DAB	Multi-resonant	Series resonant	CFFB/SAHB S-PPC
DC bus and battery terminals	Voltage-fed	Voltage-fed	Voltage-fed	Current-fed
Modulation	Phase shift + PWM	Pulse frequency	PWM + Phase shift	PWM + Phase shift
Morphing capability	Turns ratio/Inverter	Resonant tank	Inverter/rectifier	Turns ratio
Possible Confs.	4	3	4	3
Switches (S) + diodes (D)	$10S + 2D$	$12S$	$8S + 2D$	$16S$
Transformers (T)	$1T$ (three windings)	$1T$ (two windings)	$1T$ (two windings)	$1T$ (three windings)
Soft-switching	ZVS/ZCS	ZVS/ZCS	ZVS/ZCS	ZCS/ZVS
Active power flow behavior	Unidirectional	Bidirectional	Unidirectional	Bidirectional
Active power processed	Full	Full	Full	Partial
DC bus voltage	$350 - 550$ V	400 V	400 V	$320 - 380$ V
Battery voltage	$150 - 450$ V	$160 - 400$ V	$200 - 500$ V	$240 - 400$ V
Switching frequency	100 kHz	$80 - 180$ kHz	100 kHz	50 kHz
Power level	10 kW	1 kW	2.5 kW	2.2 kW

to just *ten* discrete devices. In this new technology, dual-gate ac switches are integrated into a single chip on the wafer, simplifying packaging and improving performance [16].

IV. CONCLUSION

This paper proposed a topology-morphing SIPO S-PPC for a step-up/down OBC, featuring a scheme that enables selection between conventional ac charging and integration with dc buildings. The bidirectional CFFB/SAHB S-PPC employs a three-leg switch configuration to morph its transformer primary winding, achieving three distinct turns ratios designed to reduce circulating currents. Additionally, full-range soft-switching is achieved for all switches. Simulation results align with the theoretical analysis and validate the proposed approach.

This paper extends the authors' previous research [17] by proposing a new S-PPC for a different application context.

ACKNOWLEDGMENTS

This research was supported in part by the European Union's Horizon Europe research and innovation programme under grant agreement no. 101136131, in part by the Estonian Research Council under the grant PRG2055, by the Estonian Centre of Excellence in Foundations of the Universe (grant TK202) funded by the Estonian Ministry of Education and Research, in part by the Coordination for the Improvement of Higher Education Personnel – Brazil (CAPES/PROEX) – Finance Code 001, and in part by the National Institute of Science and Technology in Distributed Generation (INCT-GD) – CNPq processes under Grants 309513/2021-9, 407654/2021-6, and 405054/2022-0, CAPES process under Grant 23038.000776/2017-54, and FAPERGS under Grant 17/2551-0000517-1.

Views and opinions expressed in this document are those of the authors only and do not necessarily reflect those of the European Union or the European Climate, Infrastructure and Environment Executive Agency. Neither the European Union nor the granting authority can be held responsible for them.

REFERENCES

[1] M. Yilmaz and P. T. Krein, "Review of battery charger topologies, charging power levels, and infrastructure for plug-in electric and hybrid vehicles," *IEEE Trans. Power Electron.*, vol. 28, no. 5, pp. 2151–2169, May 2013.

[2] D. Shu and H. Wang, "An ultrawide output range LLC resonant converter based on adjustable turns ratio transformer and reconfigurable bridge," *IEEE Trans. Ind. Electron.*, vol. 68, no. 8, pp. 7115–7124, Aug. 2021.

[3] H. Li, Z. Zhang, S. Wang, J. Tang, X. Ren, and Q. Chen, "A 300-kHz 6.6-kW SiC bidirectional *LLC* onboard charger," *IEEE Trans. Ind. Electron.*, vol. 67, no. 2, pp. 1435–1445, Feb. 2020.

[4] N. G. F. dos Santos, A. Toebe, P. H. B. Löbler, L. Schuch, M. L. d. S. Martins, and C. Rech, "A high-efficient single-switch switched-capacitor partial power converter for on-board chargers," *IEEE Trans. Power Electron.*, vol. 39, no. 11, pp. 15 269–15 280, Nov. 2024.

[5] E. L. Carvalho *et al.*, "P3R: Partial power postregulated grid-forming converter for prosumer dc buildings," *IEEE Trans. Ind. Electron.*, vol. 72, no. 2, pp. 1628–1637, Feb. 2025.

[6] J. Anzola *et al.*, "Performance improvement of a silicon partial power converter over a silicon carbide full power converter," *IEEE Trans. Transport. Electrific.*, vol. 10, no. 1, pp. 1680–1691, Mar. 2024.

[7] R. Carmona *et al.*, "High power density electric vehicle powertrain based on a T-type DAB partial power dc–dc converter," in *Proc. 2023 IEEE 8th So. Power Electron. Conf. and 17th Braz. Power Electron. Conf. (SPEC/COBEP)*, Nov. 2023, pp. 1–6.

[8] C. A. F. Freitas, P. Bartholomeus, X. Margueron, and P. Le Moigne, "Partial power converter for electric vehicle hybrid energy storage system using a controlled current source cascade architecture," *IEEE Access*, vol. 12, pp. 150 898–150 913, Oct. 2024.

[9] S. Rivera *et al.*, "Partial-power converter topology of type II for efficient electric vehicle fast charging," *IEEE Trans. Emerg. Sel. Topics Power Electron.*, vol. 10, no. 6, pp. 7839–7848, Dec. 2022.

[10] N. G. F. dos Santos *et al.*, "A review of series-connected partial power converters for dc–dc applications," *IEEE Trans. Emerg. Sel. Topics Power Electron.*, vol. 10, no. 6, pp. 7825–7838, Dec. 2022.

[11] S. Wang *et al.*, "Multifunction capability of SiC bidirectional portable chargers for electric vehicles," *IEEE Trans. Emerg. Sel. Topics Power Electron.*, vol. 9, no. 5, pp. 6184–6195, Oct. 2021.

[12] X.-F. Cheng, C. Liu, D. Wang, and Y. Zhang, "State-of-the-art review on soft-switching technologies for non-isolated dc–dc converters," *IEEE Access*, vol. 9, pp. 119 235–119 249, Aug. 2021.

[13] D. Wang *et al.*, "Structure-reconfigurable wide gain series resonant converter for on-board charger," *IEEE Trans. Circuits Syst. I, Regul. Pap.*, vol. 72, no. 4, pp. 1951–1961, Apr. 2025.

[14] R. Reddy and M. Das, "A reconfigurable bidirectional dc–dc converter with integrated battery heating for electric vehicle applications," *IEEE Trans. Emerg. Sel. Topics Ind. Electron.*, vol. 4, no. 4, pp. 1181–1191, Oct. 2023.

[15] M. A. H. Rafi and J. Bauman, "High-efficiency variable turns-ratio semi-dual active bridge converter for a dc fast charging station with energy storage," *IEEE Trans. Transport. Electrific.*, vol. 9, no. 3, pp. 3918–3935, Sept. 2023.

[16] V. Veliadis, "Monolithic bidirectional WBG switches rekindle power electronics technology [expert view]," *IEEE Power Electron. Mag.*, vol. 10, no. 1, pp. 71–75, Mar. 2023.

[17] N. G. F. dos Santos, J. R. R. Zientarski, and M. L. d. S. Martins, "A ZCS/ZVS dc–dc partial power converter with reconfigurable H-bridge and variable turns ratio for an integrated on-board charger," *IEEE Trans. Power Electron.*, vol. 39, no. 10, pp. 13 916–13 933, Oct. 2024.